Ionic guest in ionic host: ionosilica ionogel composites via ionic liquid confinement in ionosilica supports

Nicole Abdou, Bruno Alonso, Nicolas Brun, Périne Landois, Andreas Taubert, Peter Hesemann, Ahmad Mehdi

Ionic Guest in Ionic Host: Ionosilica Ionogel Composites *via* Ionic Liquid Confinement in Ionosilica Supports

Nicole Abdou[1], Bruno Alonso[1], Nicolas Brun[1], Périne Landois[2], Andreas Taubert[3], Peter Hesemann[1], Ahmad Mehdi[1]**

[1] ICGM, Univ Montpellier, CNRS, ENSCM, Montpellier, France.

[2] Laboratoire Charles Coulomb, Univ Montpellier, CNRS, Montpellier, France.

[3] Institute of Chemistry, University of Potsdam, Karl-Liebknecht-Str. 24-25, D-14476 Potsdam, Germany.

KEYWORDS

Ionosilica, ionogels, sol-gel process, confinement, solid-state NMR spectroscopy, ionic conductivity.

ABSTRACT

Ionosilica ionogels, *i.e.* composites consisting of an ionic liquid (IL) guest confined in an ionosilica host matrix, were synthesized via a non-hydrolytic sol-gel procedure from a *tris*-trialcoxysilylated amine precursor using the IL [BMIM]NTf_2 as solvent. Various ionosilica ionogels were prepared starting from variable volumes of IL in the presence of formic acid. The resulting brittle and nearly colourless monoliths are composed of different amounts of IL guests confined in an ionosilica host as evidenced *via* thermogravimetric analysis, FT-IR, and ^{13}C CP-MAS solid-state NMR spectroscopy. In the following, we focused on confinement effects between the ionic host and guest. Special host-guest interactions between the IL guest and the ionosilica host were evidenced by ^{1}H solid-state NMR, Raman spectroscopy, and broadband dielectric spectroscopy (BDS) measurements. The three techniques indicate a strongly reduced ion mobility in the ionosilica ionogel composites containing small volume fractions of confined IL, compared to conventional silica-based ionogels. We conclude that the ionic ionosilica host stabilizes an IL layer on the host surface; this then results in a strongly reduced ion mobility compared to conventional silica hosts. The ion mobility progressively increases for systems containing higher volume fractions of IL and finally reaches the values observed in conventional silica based ionogels. These results therefore point towards strong interactions and confinement effects between the ionic host and the ionic guest on the ionosilica surface. Furthermore, this approach allows confining high volume fractions of IL into self-standing monoliths while preserving high ionic conductivity. These effects may be of interest in domains where IL phases must be anchored on solid support to avoid leaching or IL spilling, *e.g.*, in catalysis, in gas separation/sequestration devices or for the elaboration of solid electrolytes for (lithium-ion) batteries and supercapacitors.

Introduction

Ionic liquids (ILs) are molten salts displaying melting temperatures lower than ca. 100°C. ILs are composed entirely of organic cations and organic or inorganic anions. Due to their unique physical and physico-chemical properties, ILs have been a subject of intense research and have been proposed for various applications, *e.g.* for energy storage,[1] catalysis,[2, 3] gas adsorption,[4] and so on. The combination of the advantageous properties of many ILs such as rather high ion conductivities over large temperature ranges (including very low temperatures), large liquidus ranges, low flammability, and high electrochemical stability has led to numerous prototypes or applications in various technologies.

However, one of the key issues is the fact that ILs are liquid. As a result, incorporation of the IL into devices like batteries or membranes is necessary. One solution to solve this problem is the use of ionogels (IGs) rather than pure ILs. IGs are composites of an IL guest that is immobilized within a solid host matrix. Indeed, IGs were thoroughly investigated in the last decade for their polyvalence that combines the properties of ILs with those of the host matrix.[5-7] In these IGs, the confinement of ILs within a solid host matrix modifies their physical properties compared to the bulk. The spatial confinement together with the interactions between confined IL and pore walls, the arrangement (ionic orientation and layer structure), physicochemical properties (diffusion coefficient, viscosity, dielectric relaxation, ionic conductivity, phase transitions, and thermal stability) and gas solubility of confined ILs significantly differ from those of the corresponding neat ILs.[8] In this latter area, Baltus *et al*. reported that both solubility and diffusivity of carbon dioxide are enhanced in ionic liquids that are confined within a porous ceramic support when compared to ionic liquids in bulk.[9] Harmanli *et al*. recently described 'giant' nitrogen uptake in ILs confined in carbon pores and attributed this effect to 'frustrated packing' of the ionic species

within the pores, thus generating free volume capable to host molecular nitrogen.[10] The impact of spatial confinement and interfacial interaction of confined ILs within a solid host matrix was also demonstrated on ionic transport properties.[11] For instance, Vereecken *et al*. suggested an optimized pore size of ca. 30 nm to maximize the so-called 'surface conduction promotion effect' while minimizing the detrimental effect of pore confinement on lithium-ion conduction.[12] All these examples highlight that confinement effects strongly modify the physico-chemical properties of confined ILs with respect to the bulk.

Besides the judicious choice of suitable ILs, the design of a suitable host material for each IL is of prime importance for the elaboration of ionogels for advanced applications. There is thus a need for a suitable scaffold capable to immobilize ILs and to prevent IL leaching and spilling while maintaining or even improving IL characteristics in the solid device. The requirements for such a 'good' scaffold are therefore multifold. An ideal IG scaffold should (1) maintain the mechanical and chemical stability during application; (2) have a high specific surface area and large pore volume to hold a high IL load; (3) have a continuous pore structure for continuous transport and diffusion within the IG; (4) allow interaction with the IL, either to enhance ion mobility (*i.e.* conductivity), or to stabilize the incorporated IL to prevent leaching, in particular for applications in catalysis; and (5) should be able to confine a high amount of IL while maintaining high mechanical stability and robustness. Various materials have been used as host matrix, including organic polymers (PMMA, PDMS),[13] carbon nanotubes (CNTs),[14] metal-organic frameworks (MOFs),[15] or metal oxides (SiO_2, TiO_2, SnO_2). [16, 17] In this context, silica is the most common host matrix, as it offers the highest textural and morphological polyvalence.[17-19] Sol-gel chemistry allows for the synthesis of a virtually unlimited number of different silica materials with well-defined and finely adjustable pore arrangements, pore sizes and size distributions, symmetries, and

chemical functionalities.[20] Sol-gel chemistry therefore offers numerous possibilities for the design of silica scaffolds with adjustable textures, architectures, morphologies, and interface properties.

In order to tune the properties of IGs, the control over the host-guest interactions between IL guest and solid scaffold host is crucial. In this work, we describe for the first time the use of ionosilicas as host material for the encapsulation of ILs. Ionosilicas are organosilicas that are exclusively constituted of ionic building blocks.[21-23] Ionosilicas combine the morphological versatility of silica-based materials with the chemical polyvalence of ILs,[24] and open up fundamentally new opportunities in the area of materials design. So far, ionosilicas have mainly been investigated for their interesting anion exchange properties,[25-27] and as drug carrier vehicles and innovative theranostic nano-tools for applications in the biomedical field.[28-30]

Herein, we focused on the elaboration of ionosilica IGs, *i.e.* composites consisting of ILs confined in an ionosilica matrix, that is, materials that are only composed of ionic building blocks. As ionosilicas contain a high number of chemically linked ionic groups, we anticipate a high affinity of the ILs towards the ionosilica support matrix, with amplified confinement effects of the encapsulated ILs. Ionosilica IGs constituted of different host/guest weight ratios were investigated by means of solid-state NMR and Raman spectroscopy together with broadband dielectric spectroscopy (BDS) measurements. The comparison of the ionosilica IGs with conventional silica based ionogels highlights the particular ability of ionosilicas for IL encapsulation and displays clear confinement effects of the IL guest within the ionosilica host. Our work points the particular position of these all-ionic composite materials in the area of IGs. Whereas poly(ionic liquid)/IL composites have already been reported and investigated as efficient carbon dioxide sequestrating phases [31, 32] and for electrochemical applications,[33] ionosilica/IL composites are a completely unexplored field yet.

Results and discussion

We firstly performed the synthesis of various ionosilica IGs. The one-pot synthesis was highly straightforward and involved only the use of three components: the ionosilica precursor **TTA**, formic acid, and the IL [BMIM]NTf_2. The ionosilica matrix was formed *via* a non-hydrolytic sol-gel procedure from the *tris* (3(trimethoxysilyl) propyl) amine precursor **TTA** (Figure 1a). The reactions were performed in IL medium, namely 1-butyl-3-methylimidazolium *bis*(trifluoromethylsulfonyl)imide, [BMIM]NTf_2. The ionosilica IGs $\mathbf{TS}_{\mathbf{x}}^{\mathbf{IL}}$,where x is the volume of the IL used, were obtained under water-free conditions using the formic acid route.[16, 34] The effect of the IL loading on the confinement of [BMIM]NTf_2 was thoroughly studied and compared with a purely inorganic silica matrix, obtained from TMOS instead of **TTA**.

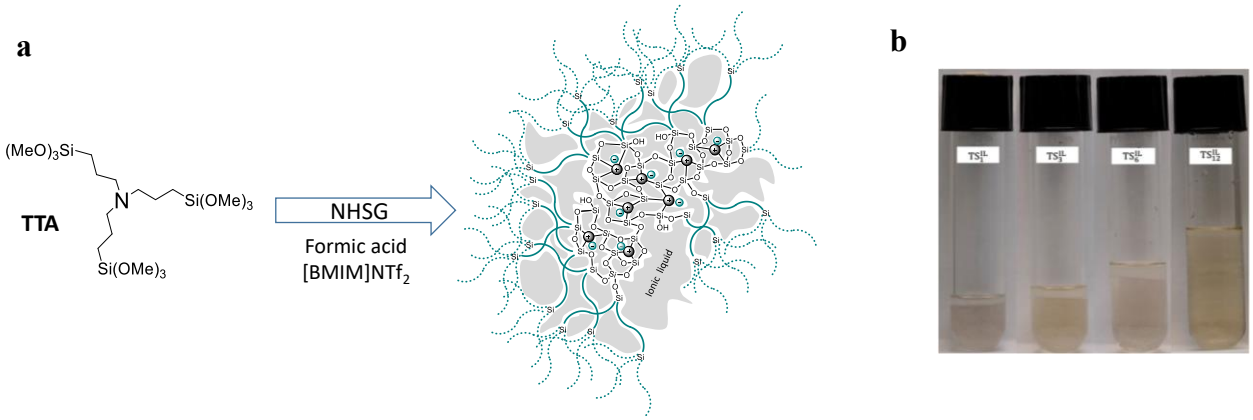

Figure 1. (a) Schematic synthesis of ionosilica ionogels; (b) photograph of the ionosilica ionogel monoliths with different IL volumes.

Four monoliths were prepared using different volumes of [BMIM]NTf_2 while keeping the quantity of ionosilica precursor **TTA** constant. For comparison, a fifth material was synthesized under identical reaction conditions using TMOS as silica precursor.[7] The exact reactant quantities

in the different trials are given in table 1. Colorless monoliths (Figure 1b) formed after several hours at room temperature. It should be mentioned that increasing quantities of IL in the reaction medium increase the gelation time of the ionosilica network, nevertheless without exceeding 24 hours for the monolith with the maximum amount of IL (*i.e.*, 12 mL). Under the given standard conditions, the quantity of the used IL cannot exceed the 12 mL, as for higher quantities, the final material displayed insufficient mechanical stability and the resulting monolith broke down to form small fragments. Figure 1b shows the as-synthesized ionosilica IG monolith reaction mixture after gelation in different volumes of IL. The final $\mathbf{TS_x^{IL}}$ were obtained after drying at 80°C under atmospheric pressure overnight and then 2 hours under vacuum (0.01 mbar).

Table 1. Used quantities for the synthesis of ionosilica ionogels.

	Precursor			[BMIM]NTf_2		HCOOH
		m(g)	n(mol)	V_0(mL)	n(mol)	V(mL)
$\boldsymbol{TS_1^{IL}}$	TTA	3.0	0.006	1	0.003	2.0
$\boldsymbol{TS_3^{IL}}$	TTA	3.0	0.006	3	0.010	2.0
$\boldsymbol{TS_6^{IL}}$	TTA	3.0	0.006	6	0.020	2.0
$\boldsymbol{TS_{12}^{IL}}$	TTA	3.0	0.006	12	0.041	2.0
$\boldsymbol{TMOS_1^{IL}}$	TMOS	2.7	0.018	3	0.010	2.7

Ionosilica monoliths of variable dimensions are formed as a function of the used IL amount. The formation of the 3D ionosilica network was confirmed *via* solid state ^{29}Si one pulse (OP) NMR spectroscopy (Figure S1) by the presence of the two signals at -58 and -68 ppm that can be attributed to silicon centers in T^2 and T^3 environments, where T^2 represents $RSi(OSi)_2(OR)_1$ centers, whereas T^3 indicates silicon in a fully condensed $R\underline{Si}(OSi)_3$-environment. The more IL

was used, the larger the dimensions of the formed $\mathbf{TS_x^{IL}}$ monoliths, thus suggesting that the amount of confined amount of IL increases with increasing IL quantity in the hydrolysis-polycondensation mixture. The photograph of the monoliths (Figure 1b) also shows that a considerable quantity of a supernatant phase was formed. To obtain a first impression of the composition of the $\mathbf{TS_x^{IL}}$ monoliths, the supernatant phase was analyzed by liquid phase ^{1}H NMR spectroscopy (Figure S2). These liquid phases basically contained formic acid, methanol (from the hydrolysis of trimethoxysilyl groups of the **TTA** precursor), transesterification products such as methyl formate, and a fraction of the IL.[35] The quantification of the amount of IL in the supernatant phase provides information about the quantity of the IL confined in the monoliths (Table 2). We found that the amount of the confined IL depends on its quantity in the starting reaction mixture. Whereas the IL is completely retained in the ionosilica matrix in the case of $\mathbf{TS_1^{IL}}$, the amount of confined IL progressively decreases to reach a fraction of 58% in $\mathbf{TS_{12}^{IL}}$. However, the amount of IL that is incorporated within the ionosilica matrix in the monoliths increases from 1 to 7 mL while keeping the quantity of the ionosilica precursor **TTA** constant (3.0 g).

Table 2. Composition of the ionosilica ionogels.

	n_{IL}/n_P	n_{IL}/n_{Si}	[BMIM]NTf_2				
			V_0(mL)	V_f(mL)	$V_0 - V_f$	%	$V_{fraction}$
$\boldsymbol{TS_1^{IL}}$	0.60	0.20	1	1	0	100	0.48
$\boldsymbol{TS_3^{IL}}$	1.70	0.56	3	2.1	0.9	70	0.65
$\boldsymbol{TS_6^{IL}}$	3.40	1.14	6	3.8	2.2	63	0.77
$\boldsymbol{TS_{12}^{IL}}$	6.80	2.27	12	7.0	5.0	58	0.86
$\boldsymbol{TMOS_1^{IL}}$	0.56	0.56	3	3	0	100	0.84

Where n_{IL}= number of moles of IL, n_p = number of moles of precursor and n_{Si} = number of moles of Si in the precursor. V_0 = Initial used volume of IL, V_f = Retained volume of IL in the ionosilica matrix and $V_{fraction} = V_f / V_f+V_{matrix,}$ where V_{matrix} is the volume of the formed 3D silica network. The density of the matrix was measured using a gas pycnometer (i.e. δ_{matrix} = 1.58 g/ cm^3 for $\mathbf{TS_x^{IL}}$, δ_{matrix} = 1.9 g/cm^3 for $\mathbf{TMOS_1^{IL}}$).

These data suggest that the ionosilica matrix forms a network with increasing mesh dimensions with increasing IL fraction. For the monolith $\mathbf{TS_{12}^{IL}}$, we can conclude the approx. 7 mL, corresponding to 10 g of IL, are well confined in roughly 2 g of an ionosilica matrix. The final, self-supporting and brittle monolith $\mathbf{TS_{12}^{IL}}$ is therefore constituted of ca. 80 wt. % of IL. This result is astounding as conventional hosts such as silica cannot retain and stabilize such a high quantity of IL while preserving a sufficient mechanical stability.[36]

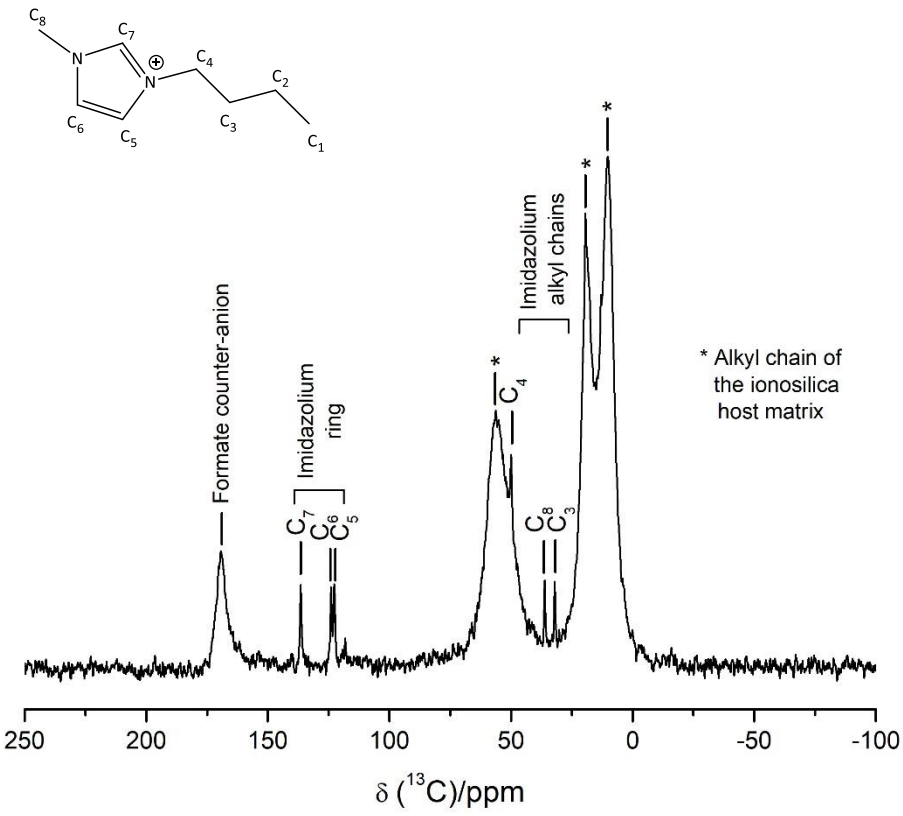

Figure 2. Solid-state ^{13}C CP NMR spectrum of the I^2SG monolith synthesized in the presence of 6 mL of IL(**TS_6^{IL}**). NMR shifts (ppm): TS alkyl chain (9.9, 19.2 and 56.7 ppm); C_3(32.1 ppm); C_4 (50.1 ppm); C_5 (122.6 ppm); C_6 (123.9 ppm); C_7 (136.4 ppm); C_8 (36.0 ppm) and formate counter-anion (166.7 ppm).

The solid-state ^{13}C CP NMR spectroscopy of the **TS_6^{IL}** confirms that the monolith is constituted only of ionosilica matrix and confined IL as indicated by the characteristic signals of the two components (Figure 2), *i.e.* the ionosilica matrix and the imidazolium cation of the [BMIM]NTf_2 ionic liquid. The presence of the IL is confirmed by the sharp signals at 32.1, 36.0, 50.1, 122.6, 123.9, and 136.4 ppm, all characteristic of the BMim-cation. The ionosilica matrix gives rise to

much larger signals at 9.9, 19.2, 56.7, and 166.7 ppm; these signals are characteristic for the alkyl chains of the **TTA** precursor and the formate counter-anion. The fact that the signal of the formate anion is rather broad indicates its low mobility and points strong interactions with the ionosilica matrix constitute of ammonium building blocks.

Additionally, the monoliths were investigated by FT-IR spectroscopy and thermogravimetric analysis (TGA). Figure 3 shows the FT-IR spectra and the thermograms of the pure ionosilica, the pure IL and the different $\mathbf{TS_x^{IL}}$ containing various amount of IL.

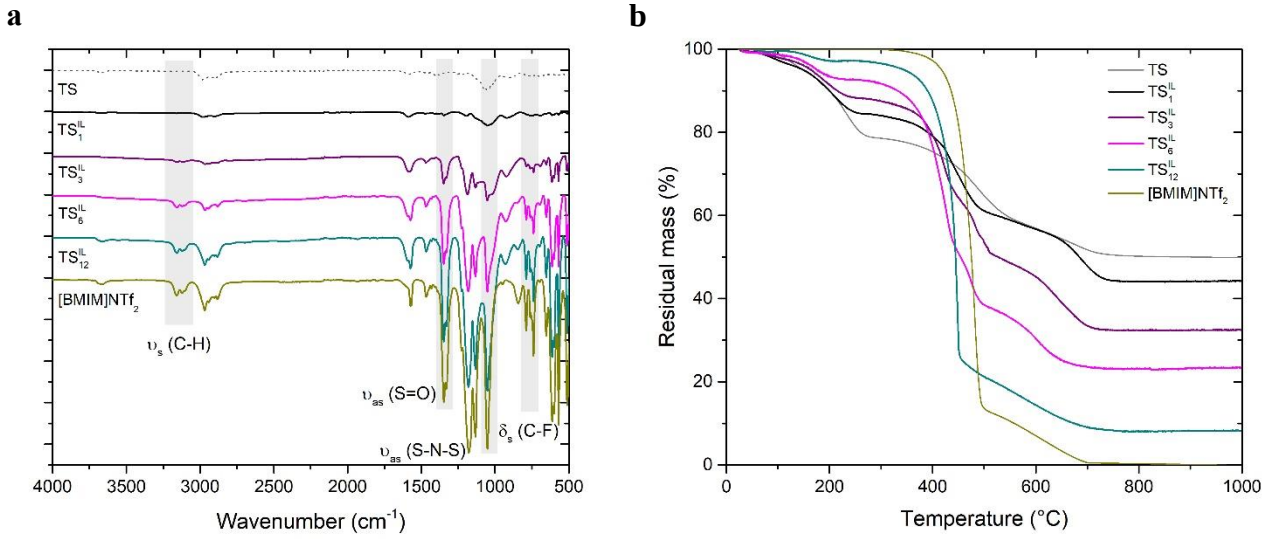

Figure 3. (a) FT-IR spectra and (b) TGA curves of I^{2}SG monoliths $\mathbf{TS_x^{IL}}$(where x is the initial volume of IL), neat TS monolith and IL.

The FT-IR spectrum of the pure ionosilica (Figure 3a) shows absorption bands between 2800-2950 cm^{-1} and at 1200 cm^{-1}. These bands stem from, C-H stretching vibrations of the alkyl chains of the ionosilica precursor and to Si-O-Si vibrations of the siloxane network, respectively. On the other hand, the spectrum of the IL shows three clearly distinguishable bands that can be attributed

to the symmetric bending of CF_3 (741 cm^{-1}), the antisymmetric stretching vibration of the S-N-S (1051 cm^{-1}) and the antisymmetric stretching vibration of the SO_2 groups (1331-1348 cm^{-1}) of the *bis*(trifluoromethylsulfonyl)imide anion. The FT-IR spectra of $\mathbf{TS_x^{IL}}$ monoliths show bands that can be attributed to both components, *i.e.* the ionosilica matrix and the confined IL. The intensities of the absorption bands depend on the ratio between both components: for IL-rich materials, the FT-IR spectra are similar to the spectra of the neat IL, whereas for IL-poor materials, the adsorption bands of the ionosilica matrix are predominant.

Similar results were obtained in TGA of the IGs. Figure 3b shows the thermograms of the pure ionosilica, the IL, and the various IGs. The higher the amount of the IL in the IGs, the more the shape of the thermograms resembles the data of the pure IL. Furthermore, the weight loss is the lowest for the IGs containing the lowest amount of IL due to the formation of the silica from the ionosilica matrix (global weight loss between 58 wt. % for $\mathbf{TS_1^{LI}}$ and 90 wt. % for $\mathbf{TS_{12}^{LI}}$), hence confirming that the highest amount on IL is confined in this material.

Overall, all analytical data confirm that $\mathbf{TS_x^{IL}}$ are all-ionic composites constituted of an IL guest confined in an ionosilica host. The amount of IL employed in the hydrolysis-polycondensation reaction mixture determines the final dimensions of the final monolith. It also determines the amount of IL confined in the ionosilica matrix. We can therefore conclude that the formed ionosilica IGs $\mathbf{TS_x^{IL}}$ are constituted of IL confined in a more or less dense ionosilica matrix

($\delta_{IS\ matrix}$ = 1.58 g/cm^3). It has to be pointed out that all $\mathbf{TS_x^{IL}}$ monoliths are brittle and self-supporting objects (Figure S3). This is a major difference compared to conventional silica-based IGs. These silica-based systems containing an identical molar amount of silicon such as material $\mathbf{TMOS_1^{IL}}$ become more and more jelly-like and are not generally self-supporting materials (Figure S4).

In order to obtain more detailed information about possible confinement effects in the ionosilica IG systems we performed ^{1}H solid-state NMR and Raman spectroscopy as well as electrochemical impedance spectroscopic measurements.

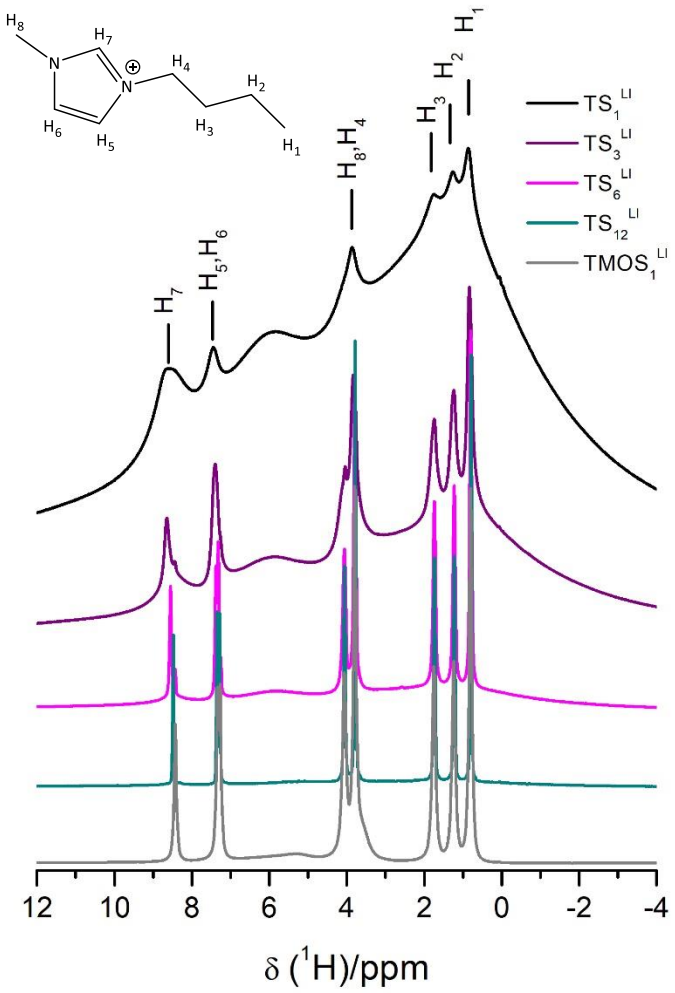

Figure 4. ^{1}H solid-state MAS NMR spectra of ground $\mathbf{TS_x^{IL}}$ and $\mathbf{TMOS_1^{IL}}$ monoliths respectively (ν_{MAS} = 24 kHz).

Figure 4 shows the ^{1}H solid-state NMR MAS spectra of ground $\mathbf{TS_x^{IL}}$ and $\mathbf{TMOS_1^{IL}}$ monoliths under rotation of 24 kHz. All spectra show the characteristic signals of the imidazolium cation with highly variable peak widths and overlapping the broader peaks of the TS matrix. The same trend is observed under static conditions (Figure S5) although the resolution is lower. The full width at half-maximum (FWHM) for the ^{1}H peaks assigned to the imidazolium cation have been estimated by spectrum fitting (Details in ESI).

Figure 5 shows (a) the variation of the FWHM as a function of the quantity of confined IL for three characteristics ^{1}H signals of the IL and (b) the variation of the FWHM of the CH_2-N signal as function of the IL $V_{fraction}$ in the $\mathbf{TS_x^{IL}}$ and $\mathbf{TMOS_1^{IL}}$ monoliths. The FWHM values decrease when the concentration of the IL increases (Figure 5a). The variations in the ^{1}H peak widths of IL can be related to variations in transverse relaxation rates dominated by the effective dipolar couplings, and notably the most intense homonuclear ^{1}H-^{1}H couplings. Therefore, the observed decrease in FWHM is explained by an increased mobility of the imidazolium cation, leading to a decrease in the effective dipolar couplings.

Furthermore, we have compared the confinement of the IL in the silica and ionosilica supports. For this purpose, we synthesized a silica IG via non-hydrolytic sol gel reaction starting from TMOS in the presence of [BMIM]NTf_2.[17, 34, 36] The amounts of TMOS, IL, and formic acid used for the synthesis of this material, $\mathbf{TMOS_1^{IL}}$, are given in Table 1. We compared the spectra of the conventional silica ionogel with those of three ionosilica ionogels ($\mathbf{TS_1^{IL}}$, $\mathbf{TS_3^{IL}}$ **and** $\mathbf{TS_{12}^{IL}}$) as they contain a similar molar amount of precursor ($\mathbf{TS_1^{IL}}$ and $\mathbf{TMOS_1^{IL}}$), a similar molar amount of silicon ($\mathbf{TS_3^{IL}}$ and $\mathbf{TMOS_1^{IL}}$) or a similar volume fraction of the encapsulated ionic liquid ($\mathbf{TS_{12}^{IL}}$ and $\mathbf{TMOS_1^{IL}}$).

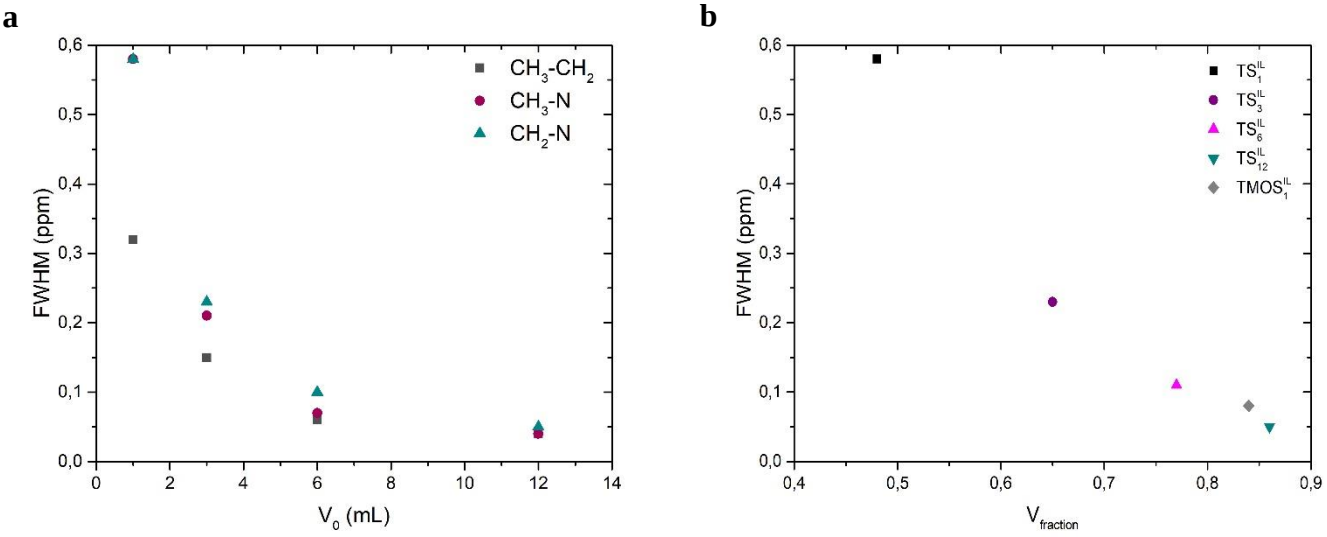

Figure 5. (a) variation of the FWHM as a function of the quantity of confined IL for three characteristics ^{1}H signals of the IL; (b) variation of the FWHM of the CH_2-N signal as function of the IL $V_{fraction}$ in the $\mathbf{TS_x^{IL}}$ and $\mathbf{TMOS_1^{IL}}$ monoliths.

Clearly, the FWHM of the signals observed in the spectra of the silica-based IG $\mathbf{TMOS_1^{IL}}$ is significantly lower than the FWHM of the signals observed in the spectra of the ionosilica IGs $\mathbf{TS_1^{IL}}$ and $\mathbf{TS_3^{IL}}$ but slightly larger than the one observed in the spectra of $\mathbf{TS_{12}^{IL}}$. The FWHM of the CH_2-N peak of $\mathbf{TS_x^{IL}}$ materials and $\mathbf{TMOS_1^{IL}}$ are represented in Table 3 and illustrated as a function of the IL volume fraction in Figure 5b. The FWHM of the signal of $\mathbf{TMOS_1^{IL}}$ of 0.08 ppm is similar compared to the FWHM found with $\mathbf{TS_6^{IL}}$ and $\mathbf{TS_{12}^{IL}}$ (0.05 ppm and 0.11 ppm, respectively). This confirms the high mobility of the IL in the silica-based IGs compared to the ionosilica IGs. The FWHM therefore reflects the mobility of IL in the various hosts and allows for the monitoring of the confinement efficiency and the strength of the interactions between host and guest. Secondly,

the higher the amount of confined IL, the higher the mobility due to the formation of larger IL domains within the ionosilica host.

These results indicate that surface localized IL (*e.g.,* in low IL content samples) strongly interacts with the ionosilica surface and therefore shows low mobility. On the other side, with increasing amounts of incorporated IL, we observed a higher amount of bulk-like IL domains displaying higher ion mobility.[37, 38]

Table 3: Data obtained via ^{1}H solid-state NMR and conductivity measurements.

	FWHM	Conductivity
	(ppm)	(S.m^{-1})
$\boldsymbol{TS_1^{IL}}$	0.58	1.5 E-05
$\boldsymbol{TS_3^{IL}}$	0.23	29 E-05
$\boldsymbol{TS_6^{IL}}$	0.11	0.028
$\boldsymbol{TS_{12}^{IL}}$	0.05	0.322
$\boldsymbol{TMOS_1^{IL}}$	0.08	0.374

The FWHM values are relative to the CH_2-N ^{1}H signal. The conductivity values are calculated based on Nyquist plots fitting using adapted equivalent circuits. (Figure S6 and Table S1)

We also addressed the IL confinement within the ionosilica hosts *via* Raman spectroscopy. Raman spectroscopy is a versatile tool to monitor the confinement of the IL in silica matrices.[34, 39-41] The Raman spectrum of bulk [BMIM]NTf_2 (Figure 6a, yellow curve) in the spectral range 1000-1300 cm^{-1} shows three characteristic bands that can be attributed to the antisymmetric vibration of the C-F bond (1036 cm^{-1}), the symmetric stretching vibration of the SO_2 (1146 cm^{-1}), and the CF_3 groups (1252 cm^{-1}) of the *bis*(trifluoromethylsulfonyl)imide anion.[42] These three

characteristic bands can also be identified in the spectra of the $\mathbf{TS_x^{IL}}$ materials (Figure 6a) confirming the presence of the IL.

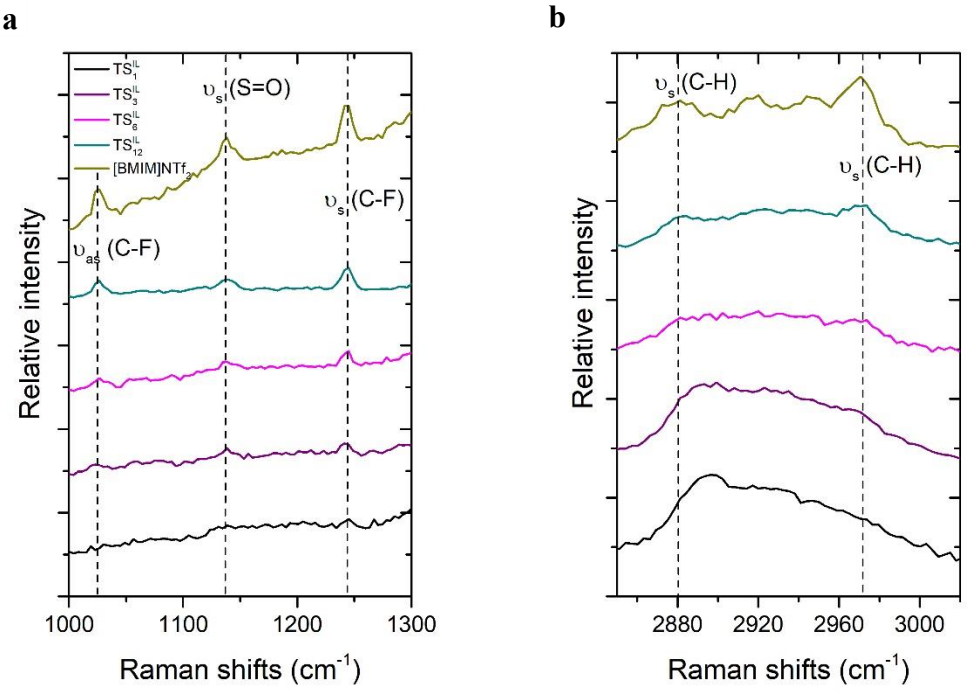

Figure 6. Raman spectra of the $\mathbf{TS_x^{IL}}$ ground monoliths and the pure IL in the range of (a) 1000-1300 cm^{-1} and (b) 2850-3100 cm^{-1} .

Figure 6b displays the Raman spectra of the neat IL and the $\mathbf{TS_x^{IL}}$ materials in the range of 2850-3100 cm^{-1}. In this part of the spectra, two bands at 2875 and 2914 cm^{-1} can be attributed to the symmetric stretching vibration of the C-H bond of the imidazolium cation.[43, 44] The intensity of the first band remains unchanged in the spectra of the whole series of the $\mathbf{TS_x^{IL}}$ materials but the shoulder at 2914 cm^{-1} appears only in the spectra of $\mathbf{TS_6^{IL}}$ and $\mathbf{TS_{12}^{IL}}$ and in the spectra of the neat IL. The presence of this shoulder thus reflects a mobile imidazolium cation and therefore indicates the presence of bulk-like IL domains. The absence of this signal in the spectra of $\mathbf{TS_1^{IL}}$ and $\mathbf{TS_3^{IL}}$

therefore indicates surface-bound imidazolium cations displaying a lower mobility. This is likely due to increased ionic interactions between the ionic guest and the ionosilica host, in agreement with the previously discussed results of the ^{1}H solid-state NMR.

To further support these results obtained by ^{1}H NMR and Raman spectroscopy, the ionic transport properties of the ionogels were determined by broadband dielectric spectroscopy (BDS) using symmetric cells with two stainless-steel electrodes.[45] Figure 7a shows the Nyquist plots obtained for the ionosilica matrices with different amounts of incorporated [BMIM]NTf_2. The corresponding ionic conductivities are collected in Table 3 and represented in Figure 7b as function of the IL $V_{fraction}$ (Table S2).

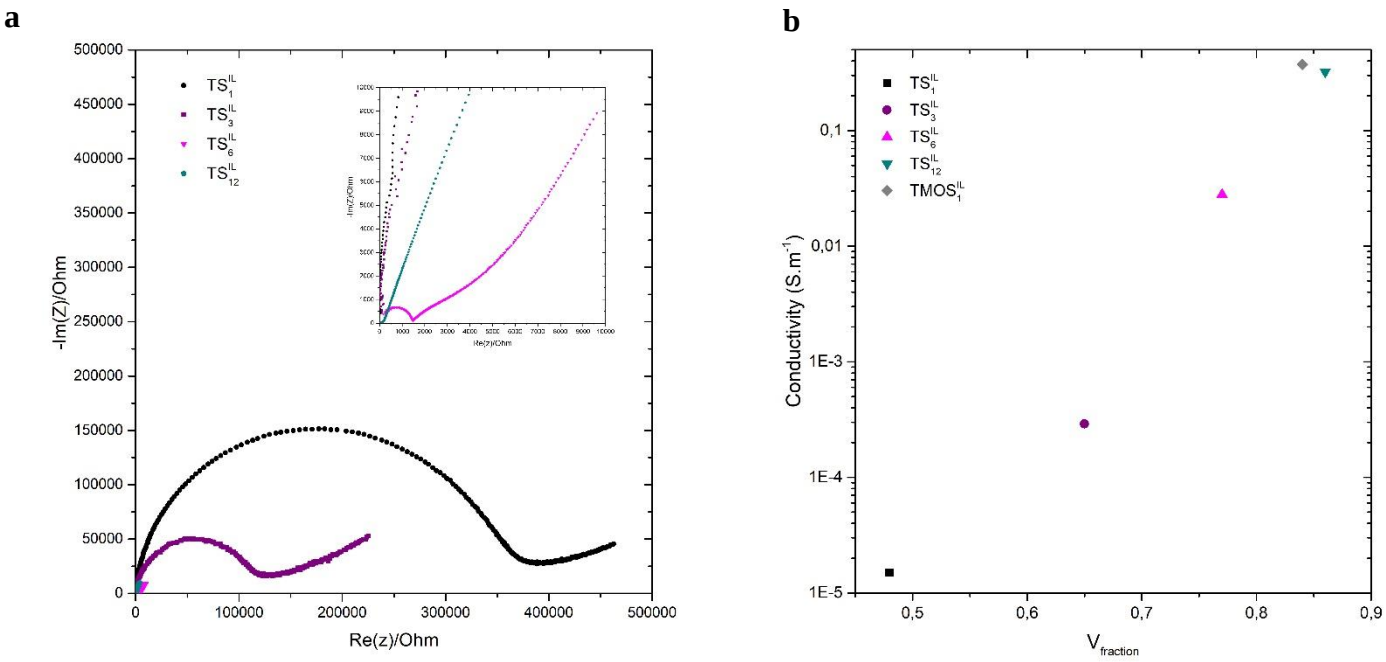

Figure 7. (a) Nyquist plots obtained for the different $\mathbf{TS_x^{IL}}$ samples using broadband dielectric spectroscopy (BDS), (b) the variation of the conductivity of the $\mathbf{TS_x^{IL}}$ and $\mathbf{TMOS_1^{IL}}$ materials as function of the IL $V_{fraction}$.

Our results show that the ionic conductivity of the ionosilica ionogels strongly depends on the quantity of encapsulated ionic liquid. The ionic conductivity increases while increasing the amount of incorporated IL. Thus, $\mathbf{TS}_{\mathbf{12}}^{\mathbf{IL}}$ displays an ion conductivity of ca. 0.32 $\mathrm{S.m^{-1}}$ that is more than four orders of magnitude higher compared to $\mathbf{TS}_{\mathbf{1}}^{\mathbf{IL}}$ (ca. 1.50E-05 $\mathrm{S.m^{-1}}$, Table 3). This feature can be associated to an increase of the mobile ionic liquid fraction in the materials that contains a larger quantity of IL, where a significant part of the encapsulated IL does not directly interact with the ionosilica matrix and therefore contributes to enhanced ionic conductivities of these phases. However, in the case of the material with the highest amount of encapsulated IL $\mathbf{TS}_{\mathbf{12}}^{\mathbf{IL}}$, the found ionic conductivity is almost equal to that of the bulk IL [BMIM]NTf_2 (0.365 $S.m^{-1}$).[46, 47]

We then compared the ionic conductivity of ionosilica ionogels to that of conventional silica based ionogels, synthesized by an analogous non-hydrolytic sol-gel method using TMOS instead of the *tris*-trialcoxysilylated amine precursor.[48] Interestingly, the ionic conductivities of all the ionosilica-based ionogels remain lower than those measured with ionogels based on conventional silica, even when the silica matrix is made with the smallest amount of IL, *i.e.* $\mathbf{TMOS}_{\mathbf{1}}^{\mathbf{IL}}$ (0.37 $\mathrm{S.m^{-1}}$, Figure S7). Furthermore, silica based ionogels display relatively constant ionic conductivity that is rather independent of the quantity of incorporated IL. The measured ionic conductivities of the $\mathbf{TMOS}_{\mathbf{x}}^{\mathrm{IL}}$ materials were very similar compared to the bulk ionic liquid (0.37 $S.m^{-1}$, Table S2), indicating that bulk IL behavior is predominant in all materials. This is a significant difference between conventional silica ionogels and ionosilica IGs. In the latter type of material, the ionic conductivity varies over four orders of magnitude in the series of materials $\mathbf{TS}_{\mathbf{1}}^{\mathbf{IL}}$ to $\mathbf{TS}_{\mathbf{12}}^{\mathbf{IL}}$ (*vide supra*) due to strong ionic interactions between ionosilica host and IL guest.

Ionosilica ionogels display modulable and adjustable electrochemical properties, contrarily to ionogels that are based on conventional silica support.

One may assume that the incorporation of ionic species in the ionosilica matrix increases the degree of electrostatic interactions in the media, which might decrease the number of mobile ions and thus the conductivity. The nature of support material therefore has deep consequences on the macroscopic properties of these materials, in particular on the ionic conductivities.

Finally, it has to be mentioned that all the ionosilica-based ionogels reported herein are self-standing monoliths, which can be easily handled, cut, and shaped. Conversely, viscous unstable gels were obtained using TMOS, even for the silica matrix made with the smallest amount of IL, *i.e.,* $\mathbf{TMOS_1^{IL}}$ (Figure 7b). We believe that this feature is critical for the incorporation of such ionogels into advanced electrochemical devices, for which the ionosilica-based ionogels reported herein might be highly advantageous.

Conclusion

In this work, ionosilica-based IGs with different amounts of confined IL have been prepared using a non-hydrolytic sol-gel process. All materials were obtained as brittle and self-standing monoliths. More specifically, ionosilica IGs can incorporate more than 80 wt. % of IL while maintaining a mechanically robust morphology. This is a significant difference compared to conventional silica-based IGs that show jelly like morphologies for similar molar IL/ionosilica ratios. The incorporation of an IL in an ionosilica host increases electrostatic interaction between host and guest. This results in reduced ion mobility and conductivity compared to conventional silica IGs, that can however be controlled via the amount of incorporated IL. Contrarily to silica based ionogels, the ionic conductivity of ionosilica based ionogels strongly depends on the quantity of encapsulated IL. As a consequence, the ion conductivity in these latter phases increase over four orders of magnitude by increasing the amount of encapsulated IL within the ionosilica matrices. We attribute this result to strongly increased host-guest interactions, resulting in strongly reduced ion mobilities in the case of ionosilica ionogels containing small quantities of IL. Contrarily to silica based ionosilicas, ionosilica based ionosilicas therefore display variable electrochemical properties. We believe that the obtained ionosilica IGs are highly polyvalent materials with adaptable properties that may find applications in various fields as different as electrocatalysis, gas absorption, electrochemistry, and energy storage. Our work therefore opens the route to other functional ionosilica IG combinations for specific applications in various domains.

Supporting Information

Electronic supplementary information (ESI) available. See DOI: 10.1039/xxxx:

- Experimental details
- Apparatus and analytical procedures
- Supplementary solid and liquid NMR spectra
- Photographs of ionogels
- ^{1}H NMR MAS spectra monoliths under static conditions
- Fitted NMR spectra using the DmFit software
- Nyquist plots obtained for the different silica-based ionogels samples

Acknowledgements

We thank for the excellent technical assistance of Philippe Gaveau and Emmanuel Fernandez for solid state NMR measurements and Amine Geneste for TGA measurements.

Author Contributions

The manuscript was written through contributions of all authors. All authors have given approval to the final version of the manuscript.

Notes

The authors declare no competing financial interest.

References

1. M. Watanabe, M. L. Thomas, S. G. Zhang, K. Ueno, T. Yasuda and K. Dokko, Application of Ionic Liquids to Energy Storage and Conversion Materials and Devices, *Chem. Rev.*, 2017, **117**, 7190-7239.
2. V. I. Parvulescu and C. Hardacre, Catalysis in ionic liquids, *Chem. Rev.*, 2007, **107**, 2615-2665.
3. J. P. Hallett and T. Welton, Room-Temperature Ionic Liquids: Solvents for Synthesis and Catalysis. 2, *Chem. Rev.*, 2011, **111**, 3508-3576.
4. M. Hasib-ur-Rahman, M. Siaj and F. Larachi, Ionic liquids for CO2 capture—Development and progress, *Chemical Engineering and Processing: Process Intensification*, 2010, **49**, 313-322.
5. S. Zhang, J. Zhang, Y. Zhang and Y. Deng, Nanoconfined Ionic Liquids, *Chem. Rev.*, 2017, **117**, 6755-6833.
6. M. P. Singh, R. K. Singh and S. Chandra, Ionic liquids confined in porous matrices: Physicochemical properties and applications, *Prog. Mater. Sci.*, 2014, **64**, 73-120.
7. J. Le Bideau, L. Viau and A. Vioux, Ionogels, ionic liquid based hybrid materials, *Chem. Soc. Rev.*, 2011, **40**, 907-925.
8. R. Göbel, A. Friedrich and A. Taubert, Tuning the phase behavior of ionic liquids in organically functionalized silica ionogels, *Dalton Trans.*, 2010, **39**, 603-611.
9. L. A. Banu, D. Wang and R. E. Baltus, Effect of Ionic Liquid Confinement on Gas Separation Characteristics, *Energ. Fuel*, 2013, **27**, 4161-4166.
10. I. Harmanli, N. V. Tarakina, M. Antonietti and M. Oschatz, "Giant" Nitrogen Uptake in Ionic Liquids Confined in Carbon Pores, *J. Am. Chem. Soc.*, 2021, **143**, 9377-9384.
11. A. Guyomard-Lack, B. Said, N. Dupre, A. Galarneau and J. Le Bideau, Enhancement of lithium transport by controlling the mesoporosity of silica monoliths filled by ionic liquids, *New J. Chem.*, 2016, **40**, 4269-4276.
12. A. Sagara, H. Yabe, X. Chen, B. Put, T. Hantschel, M. Mees, H. Arase, Y. Kaneko, A. Uedono and P. M. Vereecken, Interfacial Conductivity Enhancement and Pore Confinement Conductivity-Lowering Behavior inside the Nanopores of Solid Silica-gel Nanocomposite Electrolytes, *ACS Appl. Mater. Interf.*, 2021, **13**, 40543-40551.
13. P. Izak, S. Hovorka, T. Bartovsky, L. Bartovska and J. G. Crespo, Swelling of polymeric membranes in room temperature ionic liquids, *J. Membrane Sci.*, 2007, **296**, 131-138.
14. P. Simon and Y. Gogotsi, Capacitive Energy Storage in Nanostructured Carbon-Electrolyte Systems, *Acc. Chem. Res.*, 2013, **46**, 1094-1103.
15. A. Singh, R. Vedarajan and N. Matsumi, Modified Metal Organic Frameworks (MOFs)/Ionic Liquid Matrices for Efficient Charge Storage, *J. Electrochem. Soc.*, 2017, **164**, H5169-H5174.
16. S. Dai, Y. H. Ju, H. J. Gao, J. S. Lin, S. J. Pennycook and C. E. Barnes, Preparation of silica aerogel using ionic liquids as solvents, *Chem. Commun.*, 2000, 243-244.
17. M.-A. Neouze, J. Le Bideau, P. Gaveau, S. Bellayer and A. Vioux, Ionogels, New Materials Arising from the Confinement of Ionic Liquids within Silica-Derived Networks, *Chem. Mater.*, 2006, **18**, 3931-3936.
18. A. Vioux, L. Viau, S. Volland and J. Le Bideau, Use of ionic liquids in sol-gel; ionogels and applications, *CR Chim.*, 2010, **13**, 242-255.

19. R. Göbel, P. Hesemann, J. Weber, E. Möller, A. Friedrich, S. Beuermann and A. Taubert, Surprisingly high, bulk liquid-like mobility of silica-confined ionic liquids, *Phys. Chem. Chem. Phys.*, 2009, **11**, 3653-3662.
20. A. Mehdi, C. Reye and R. Corriu, From molecular chemistry to hybrid nanomaterials. Design and functionalization, *Chem. Soc. Rev.*, 2011, **40**, 563-574.
21. T. P. Nguyen, P. Hesemann, T. M. Linh Tran and J. J. E. Moreau, Nanostructured polysilsesquioxanes bearing amine and ammonium groups by micelle templating using anionic surfactants, *J. Mater. Chem.*, 2010, **20**, 3910-3917.
22. S. El Hankari, B. Motos-Perez, P. Hesemann, A. Bouhaouss and J. J. E. Moreau, Pore size control and organocatalytic properties of nanostructured silica hybrid materials containing amino and ammonium groups, *J. Mater. Chem.*, 2011, **21**, 6948-6955.
23. P. Hesemann, T. P. Nguyen and S. El Hankari, Precursor Mediated Synthesis of Nanostructured Silicas: From Precursor-Surfactant Ion Pairs to Structured Materials, *Materials*, 2014, **7**, 2978-3001.
24. U. D. Thach, P. Trens, B. Prelot, J. Zajac and P. Hesemann, Tuning the Interfacial Properties of Mesoporous Ionosilicas: Effect of Cationic Precursor and Counter Anion, *J. Phys. Chem. C*, 2016, **120**, 27412-27421.
25. U. D. Thach, P. Hesemann, G. Yang, A. Geneste, S. Le Caër and B. Prelot, Ionosilicas as efficient sorbents for anionic contaminants: Radiolytic stability and ion capacity, *J. Colloid. Interf. Sci.*, 2016, **482**, 233-239.
26. R. Bouchal, I. Miletto, U. D. Thach, B. Prelot, G. Berlier and P. Hesemann, Ionosilicas as efficient adsorbents for the separation of diclofenac and sulindac from aqueous media, *New J. Chem.*, 2016, **40**, 7620-7626.
27. U. D. Thach, B. Prelot, S. Pellet-Rostaing, J. Zajac and P. Hesemann, Surface Properties and Chemical Constitution as Crucial Parameters for the Sorption Properties of Ionosilicas: The Case of Chromate Adsorption, *ACS Appl. Nano Mater.*, 2018, **1**, 2076-2087.
28. R. Bouchal, M. Daurat, M. Gary-Bobo, A. Da Silva, L. Lesaffre, D. Aggad, A. Godefroy, P. Dieudonne, C. Charnay, J. O. Durand and P. Hesemann, Biocompatible Periodic Mesoporous Ionosilica Nanoparticles with Ammonium Walls: Application to Drug Delivery, *ACS Appl. Mater. Interf.*, 2017, **9**, 32018-32025.
29. M. Daurat, S. Rahmani, R. Bouchal, A. Akrout, J. Budimir, C. Nguyen, C. Charnay, Y. Guari, S. Richeter, L. Raehm, N. Bettache, M. Gary-Bobo, J. O. Durand and P. Hesemann, Organosilica Nanoparticles for Gemcitabine Monophosphate Delivery in Cancer Cells, *ChemNanoMat*, 2019, **5**, 888-896.
30. B. Mezghrani, L. M. A. Ali, S. Richeter, J. O. Durand, P. Hesemann and N. Bettache, Periodic Mesoporous Ionosilica Nanoparticles for Green Light Photodynamic Therapy and Photochemical Internalization of siRNA, *ACS Appl. Mater. Interf.*, 2021, **13**, 29325-29339.
31. S. Y. Zhang, Q. Zhuang, M. Zhang, H. Wang, Z. M. Gao, J. K. Sun and J. Y. Yuan, Poly(ionic liquid) composites, *Chem. Soc. Rev.*, 2020, **49**, 1726-1755.
32. L. C. Tome and I. M. Marrucho, Ionic liquid-based materials: a platform to design engineered CO2 separation membranes, *Chem. Soc. Rev.*, 2016, **45**, 2785-2824.
33. Y. M. Kim, W. Y. Choi, J. H. Kwon, J. K. Lee and H. C. Moon, Functional Ion Gels: Versatile Electrolyte Platforms for Electrochemical Applications, *Chem. Mater.*, 2021, **33**, 2683-2705.

34. A. Martinelli and L. Nordstierna, An investigation of the sol-gel process in ionic liquid-silica gels by time resolved Raman and 1H NMR spectroscopy, *Phys. Chem. Chem. Phys.*, 2012, **14**, 13216-13223.
35. A. Vioux, Nonhydrolytic Sol−Gel Routes to Oxides, *Chem. Mater.*, 1997, **9**, 2292-2299.
36. J. Le Bideau, P. Gaveau, S. Bellayer, M. A. Neouze and A. Vioux, Effect of confinement on ionic liquids dynamics in monolithic silica ionogels: 1H NMR study, *Phys. Chem. Chem. Phys.*, 2007, **9**, 5419-5422.
37. B. Coasne, L. Viau and A. Vioux, Loading-Controlled Stiffening in Nanoconfined Ionic Liquids, *J. Phys. Chem. Lett.*, 2011, **2**, 1150-1154.
38. G. Ori, F. Villemot, L. Viau, A. Vioux and B. Coasne, Ionic liquid confined in silica nanopores: molecular dynamics in the isobaric-isothermal ensemble, *Mol. Phys.*, 2014, **112**, 1350-1361.
39. D. Aidoud, D. Guy-Bouyssou, D. Guyomard, J. L. Bideau and B. Lestriez, Photo-Polymerized Organic Host Network of Ionogels for Lithium Batteries: Effects of Mesh Size and of Ethylene Oxide Content, *J. Electrochem. Soc.*, 2018, **165**, A3179-A3185.
40. A. Marie, B. Said, A. Galarneau, T. Stettner, A. Balducci, M. Bayle, B. Humbert and J. Le Bideau, Silica based ionogels: interface effects with aprotic and protic ionic liquids with lithium, *Phys. Chem. Chem. Phys.*, 2020, **22**, 24051-24058.
41. S. Vavra, K. Elamin, L. Evenäs and A. Martinelli, Transport Properties and Local Structure of an Imidazole/Protic Ionic Liquid Mixture Confined in the Mesopores of Hydrophobic Silica, *J. Phys. Chem. C*, 2021, **125**, 2607-2618.
42. J. Kiefer, J. Fries and A. Leipertz, Experimental Vibrational Study of Imidazolium-Based Ionic Liquids: Raman and Infrared Spectra of 1-Ethyl-3-methylimidazolium Bis(Trifluoromethylsulfonyl)imide and 1-Ethyl-3-methylimidazolium Ethylsulfate, *Appl. Spectrosc.*, 2007, **61**, 1306-1311.
43. J. Wu, X. Zhu, H. Li, L. Su, K. Yang, X. Cheng, G. Yang and J. Liu, Combined Raman Scattering and X-ray Diffraction Study of Phase Transition of the Ionic Liquid [BMIM][TFSI] Under High Pressure, *J. Solution Chem.*, 2015, **44**, 2106-2116.
44. V. H. Paschoal, L. F. O. Faria and M. C. C. Ribeiro, Vibrational Spectroscopy of Ionic Liquids, *Chem. Rev.*, 2017, **117**, 7053-7112.
45. M. Meyer, PhD thesis, Université de Montpellier 2, 2014.
46. A. Andriola, K. Singh, J. Lewis and L. Yu, Conductivity, Viscosity, and Dissolution Enthalpy of $LiNTf_2$ in Ionic Liquid $BMINTf_2$, *J. Phys. Chem. B*, 2010, **114**, 11709-11714.
47. M. Vranes, S. Dozic, V. Djeric and S. Gadzuric, Physicochemical Characterization of 1-Butyl-3-methylimidazolium and 1-Butyl-1-methylpyrrolidinium Bis(trifluoromethylsulfonyl)imide, *J. Chem. Eng. Data*, 2012, **57**, 1072-1077.
48. A. Saminathan, S. Krishnasamy and G. Venkatachalam, Enhanced Electrochemical Performance of a Silica Bead-Embedded Porous Fluoropolymer Composite Matrix for Li-Ion Batteries, *Ing. Eng. Chem. Res.*, 2020, **59**, 21028-21038.